Tunable far infrared laser spectroscopy of van der Waals bonds: Vibration–rotation–tunneling spectra of Ar–H_2O

R. C. Cohen, Kerry L. Busarow, K. B. Laughlin, Geoffrey A. Blake,[a] M. Havenith,[b] Y. T. Lee, and R. J. Saykally

Department of Chemistry and Materials and Chemical Sciences Division, University of California and Lawrence Berkeley Laboratories, Berkeley, California 94720

(Received 31 May 1988; accepted 27 June 1988)

The first high resolution spectra of a rare gas–H_2O cluster have been observed using a tunable far infrared laser to probe the vibration–rotation–tunneling levels of Ar–H_2O formed in a continuous planar supersonic jet. The high sensitivity of this spectrometer facilitated extensive measurements of two perpendicular subbands which are assigned to transitions from the ground state to the upper component of a hydrogen exchange tunneling doublet (c-type) at 21 cm^{-1}, and to $v_{b1} = 1^+$ (b-type) at 25 cm^{-1}, the lower tunneling component of a bending vibration which is perpendicular to the tunneling coordinate. The tunneling splitting is shown to be in the range 2.5–7 cm^{-1} and the lower tunneling component of the excited bending vibration lies between 39 and 43 cm^{-1} above the ground state of the complex. The experimentally determined center-of-mass separation ($R_{c.m.} = 3.75$ Å) and harmonic stretching force constant ($k_s = 0.0134$ mdyn/Å) are compared to those of related first and second row hydrides. The large amplitude motions occurring within this complex make it difficult to establish its structure.

INTRODUCTION

The study of van der Waals clusters has been motivated by the need for a deeper understanding of the static and dynamical properties of condensed phases on a molecular level. Although numerous complexes have been studied by a wide array of techniques, a general understanding of intermolecular forces which allows one to predict the structures of weakly bound clusters, has yet to emerge. However, some simple generalizations concerning the structures of dimers have evolved. For example, in an extensive series of papers by Klemperer *et al.*,[1] ammonia has been shown to bind exclusively as a Lewis base, directing its lone pair toward its binding partner. Interestingly, no evidence has been found for hydrogen bonding by NH_3 in the gas phase.[1] In contrast to ammonia, knowledge of the structures of weakly bound complexes containing water extracted from microwave and radio frequency spectroscopy studies confirms the amphoteric behavior expected for binding with H_2O. In some complexes, viz., $(H_2O)_2$,[2,3] H_2O–HX (X = F,[4] Cl,[5] and CN[6]), H_2O–C_2H_2,[7] and H_2O–CO_2,[8] water serves as a Lewis base (hydrogen bond acceptor), while in others, viz., $(H_2O)_2$,[2,3] NH_3–H_2O,[9] H_2O–C_2H_4,[10] H_2O–CO,[11] and H_2O–NH_2CHO,[12] it serves as a Lewis acid (hydrogen bond donor). Several of the analogous H_2S clusters, H_2S–HX (X = F,[13,14] Cl,[15] Br,[16] and CN[17]), in which H_2S serves as a Lewis base, have been studied as well.

Microwave and radio frequency spectra typically sample only the ground vibrational state, making it difficult to extract significant details (i.e., anisotropy) of the global potential surface (observation of vibrational satellites of H_2O–HF[4] is a prominent exception). Many van der Waals complexes, including Ar–H_2O are presumed to exhibit potential energy surfaces which have multiple, nearly isoenergetic minima and barriers [e.g., $(HCN)_3$ exists in linear and cyclic forms[18]] at substantially different geometries. Detailed characterizations of these intermolecular potential energy surfaces (PES) are essential if we are to understand the anisotropic forces which determine the equilibrium structures of van der Waals molecules and the dynamical processes (e.g., hydrogen exchange tunneling) which take place within these clusters. With few exceptions (including the rare gas–H_2,[19,20] Ar–HCl,[21–23] and He–C_2H_2, –C_2H_4, –C_2H_6[24] dimers) our current *experimental* knowledge of intermolecular potentials is limited to isotropic functions extracted from classical experiments and molecular beam scattering studies and to inferences based on rotational spectroscopy of the ground vibrational states of molecular clusters. It is not yet possible to compute accurate anisotropic van der Waals potentials with *ab initio* methods.

Measurements of the vibrational eigenstates of the intermolecular potential clearly sample a much more extensive region of the PES than do rotational spectra in the ground vibrational level. For example, a recent study of the FIR vibration–rotation spectra of the van der Waals complex Ar–HCl by Robinson *et al.*[21–23] has led to Hutson's determination of an improved potential energy surface for this prototype anisotropic system, deduced exclusively from high resolution spectroscopic data.[25] This PES is considerably more accurate at positions on the surface far from the equilibrium geometry than its predecessor, the M5 potential.[26] Additional measurements made by Busarow *et al.*[27] will allow a considerable improvement in the PES in the

[a] Berkeley Miller Postdoctoral Fellow. Present address: Division of Geological and Planetary Sciences, California Institute of Technology 170-25, Pasadena, California 91125.

[b] Permanent address: Institut für Angewandte, Physik, Universität Bonn, Wegelerstr. 8, D-5300 Bonn 1, West Germany.

 0021-9606/88/204494-11$02.10

region of the Ar–ClH configuration. Based on the results obtained for Ar–HCl, the Ar–H_2O dimer is expected to have potential minima at both hydrogen bonded geometries [Fig. 1(a)] and at an Ar–OH_2 configuration [Fig. 1(c)]. Characterizing the relative depths of the minima at these and/or other Ar–H_2O geometries will help us in understanding the structure of other H_2O clusters, for which one or the other type of binding more obviously dominates. Toward this end, a long-term goal initiated by the present study is to extend the approach taken in the development of the improved Ar–HCl potential surface[25] to the development of potential energy surfaces for more complex topologies, in this case that of an atom–triatom system. Because excitation of the high frequency infrared bending and stretching modes of the H_2O substituent generally results in large changes in the effective van der Waals potential,[28] we have concentrated our efforts on measurement of the low frequency far infrared (FIR) vibrations of the van der Waals bonds themselves.

Existing pair potentials for the rare gas–H_2O systems have been used in the modeling of "hydrophobic" effects,[29,30] nevertheless there is surprisingly little experimental or theoretical data available for them. An *ab initio* study of the Ne– and Ar–H_2O dimers by Losonczy, Moskowitz, and Stillinger[31] predicts that these complexes have an equilibrium structure in which the rare gas atom is in a linear hydrogen bonded configuration. Calculations on He–H_2O were performed by Lischka,[32] but only at planar C_{2v} geometries. This study showed the complex to have a deeper minimum with He localized on the hydrogen side of H_2O. Later work by Kolos, Corongiu, and Clementi[33] concluded that a planar C_{2v} structure with a rare gas atom bound to the hydrogen end of H_2O was the lowest energy form of Ar–H_2O. Minima calculated along seven different directions of approach were determined to lie within 35 cm^{-1} of one another for this cluster. We note that at the same level of theory (SCF + London dispersion term), the authors did not find the secondary minimum for the Ar–HCl complex at the Ar–ClH configuration, which has since been shown to be only 28 cm^{-1} above the global minimum at the Ar–HCl configuration.[25] Hence these theoretical predictions are not expected to provide reliable information on the cluster structures.

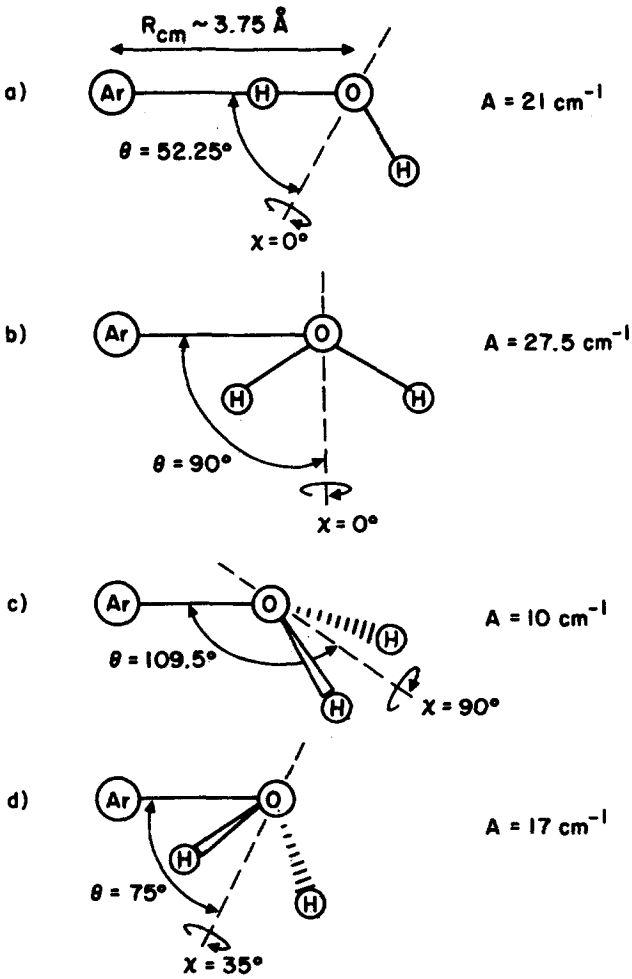

FIG. 1. Four possible structures for the Ar–H_2O dimer. These span the range of possible values for the A rotational constant. Structures (a) and (b) are constrained to be planar; (c) is a pyramidal; and (d) is the H_2O analog of the Ar–H_2S structure determined by Viswanathan and Dyke (Ref. 35).

The only detailed experimental studies of rare gas–H_2O dimers are the molecular beam scattering measurements of Bickes *et al.*[34] and Brooks *et al.*,[35] from which isotropic 12-6-type potential energy surfaces were extracted, indicating a binding energy for Ar–H_2O of 125 cm^{-1} and an equilibrium bond length of 2.9 Å. Ne–H_2O was found to be bound by 48 cm^{-1} at $R_e = 2.8$ Å and He–H_2O by 22 cm^{-1} at $R_e = 2.9$ Å. High resolution molecular beam electric resonance spectra of the homologous Ar–H_2S complex by Viswanathan and Dyke[36] has shown the C_{2v} axis of H_2S to be nearly perpendicular to the argon–sulfur bond with the hydrogens rotated 35° about the C_{2v} axis from a reference planar configuration [analogous to Fig. 1(d)]. As the authors indicate, this structure is difficult to reconcile with a linear hydrogen bonded equilibrium geometry. Since H_2O is considerably more acidic than H_2S, the Ar–H_2O complex is more likely to be hydrogen bonded. This argument parallels the experimental results for Ar–HF and Ar–HCl, viz., HF is more acidic than HCl and a much stronger hydrogen bond is found in Ar–HF than in Ar–HCl.

We report here the first spectroscopic detection of the van der Waals cluster Ar–H_2O. Vibration–rotation–tunneling (VRT) levels up to 60 cm^{-1} above the zero-point energy have been accessed and three different VRT sublevels have been identified, providing direct information on the PES over a considerable range of geometries and internal energies. The spectra presented here, and in our recent studies of Ar–HCl,[27] $(HCl)_2$,[37] and $(H_2O)_2$[38] are a result of recent advances in our ability to continuously scan over large ranges of the FIR with high sensitivity and high resolution, using state of the art developments in tunable FIR laser technology[39,40] and a newly designed continuous planar supersonic free jet.[27] We have cataloged over 250 lines in the range 17 to 28 cm^{-1}, 89 of the strongest being assigned to VRT transitions of the Ar–H_2O dimer, while others are assigned to $(H_2O)_2$.[38]

EXPERIMENTAL

FIR spectra of Ar–H_2O were measured with a tunable laser sideband spectrometer and a continuous two-dimensional free jet as a source of clusters; a schematic is shown in Fig. 2. Detailed descriptions of both the laser[39,40] and of the planar jet[27] have been given elsewhere and will only be briefly reviewed here. Ar–H_2O was formed by bubbling argon (Liquid Air, 99.99%) through distilled water at room temperature. The mixture containing argon and several Torr of water vapor was then expanded continuously through the 1.5×0.001 in. stainless steel slit. The expansion chamber was evacuated by a 2600 cfm Roots blower (Edwards EH4200) backed by two 145 cfm mechanical pumps (Edwards E2M275). The pumping speed is limited by the 40 ft. $\times$ 8 in. i.d. vacuum line connecting the chamber and the pumps to 1600 cfm. Typical operating conditions were a 900–1000 Torr backing pressure expanded into a chamber pressure of approximately 100 mTorr. Based on the measured fractional absorption of the 1_{10}–1_{01} line of $H_2{}^{18}O$ at 547.676 GHz as 1% and an assumed 5 K expansion temperature,[27] we estimate the density of water in the jet to be approximately 10^{12} cm^{-3} at the intersection with the far infrared laser beam, about 1 cm downstream from the nozzle. This yields an estimate of 10^{15} molecules/cm^{-3} for the density in the region probed by the laser. We can also estimate the density of the Ar–H_2O cluster; assuming the transition moment for the Ar–H_2O transition to be 1 D, the observed fractional absorption of the low J, K lines of 1% gives a value of approximately 10^{10} cm^{-3} for the density of the complex. As we have noted previously,[27] the planar expansion has the advantage of greatly increasing the density path length product and simultaneously reducing the Doppler linewidths by an order of magnitude relative to results obtained with conventional circular nozzles. Planar jets are also predicted[41] to facilitate clustering to a greater extent than do pinhole expansions. This combination of effects has resulted in signal-to-noise ratios exceeding 1000:1 for FIR laser spectra of the dimers Ar–HCl, $(HCl)_2$, and Ar–H_2O.

The highly monochromatic FIR radiation required for these experiments was produced by mixing the output from a longitudinally pumped FIR molecular laser with that from a multiplied YIG-tuned microwave oscillator (HP8673B) in a Schottky barrier diode (Univ. Va. No. 1E12). A 150 W, cw, line tunable CO_2 laser (Apollo Model 150) provides the infrared pump radiation which drives a 2.3 m FIR laser. Three formic acid laser lines were used in this study, at 513, 432, and 394 μm (584.3882, 692.9514, and 761.6083 GHz, respectively). The laser frequencies used in calculating absolute frequencies for the measured lines were taken from the compilation by Ignuscio *et al.*[42] By incorporating doublers into the microwave circuitry (Spacek Ka2X, Honeywell V2200N) and employing a Hughes 8001H12 traveling wave tube amplifier, the 2–26.5 GHz tuning range of the HP8673B is extended to 75 GHz. The use of a semirigid cable transmission line (Wiltron), which operates single mode to 45 GHz, has increased the sensitivity at the edges of each scanning range (22–26, 40–50, and 65–75 GHz). At high frequencies (45–75 GHz) where the microwaves are coupled onto the diode via Ka-band waveguide, the addi-

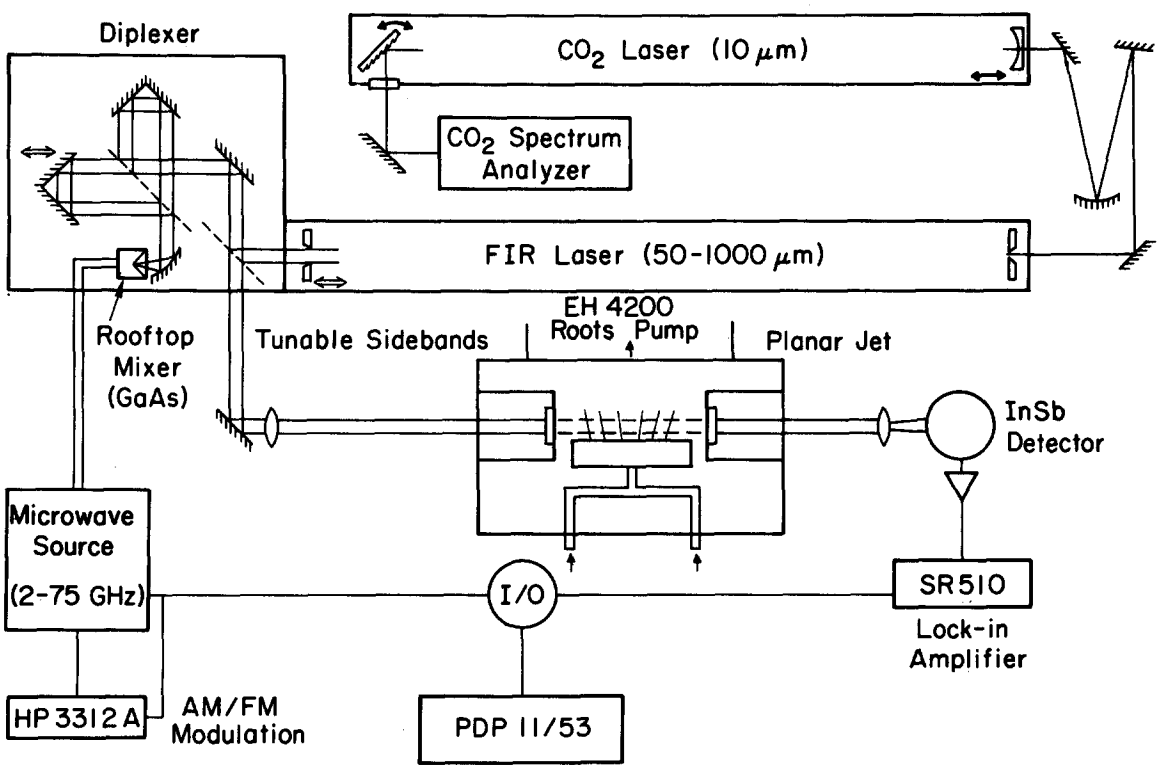

FIG. 2. Tunable far infrared laser/planar jet apparatus described in the text.

tional microwave power also facilitates longer sweeps, since the E–H tuner and backshort used to optimize the rf power matched onto the diode may be deliberately detuned to achieve power levels which are flat over a broad range of microwave frequencies. Spectra were recorded by frequency modulation of the microwave source with lock-in detection at $2f$. $2f$ detection is preferrable to $1f$ detection, since it reduces amplitude fluctuations created by modulation of the microwave source below the detector noise level. On strong laser lines, such as those used in this study, approximately 100–200 μW of tunable FIR radiation is produced, which passes directly through the supersonic expansion onto a liquid helium cooled InSb hot electron bolometer (Cochise Instruments). Minimum detectable fractional absorptions of 1 part in 10^5 for an integration time of 1 s are typical for this system.

The frequency accuracy of the spectrometer is determined by short-term jitter and long-term drift of the FIR laser. The short-term (a few minutes) frequency accuracy of the system is on the order of 10 kHz[40]; hence, when suitable standards are employed, frequencies can be determined to this level of precision, as has been demonstrated for Ar–HCl.[27] In the present work, as in our study of $(HCl)_2$,[37] we have not attempted to accurately calibrate the individual lines, as this is quite tedious, and the accuracy achieved would be beyond that which can currently contribute to the development of an intermolecular potential. As each of the lines was measured, the FIR laser frequency was "pulled" to determine which sideband it was on. The uncertainties in the absolute frequencies of the measured lines are dominated by the inaccuracy involved in the resetting of the laser to the peak of its gain curve after this "pulling." We estimate this error to be about 0.5 MHz.

ASSIGNMENT AND ANALYSIS

Eighty-nine FIR spectral lines (Tables I and II) have been measured and assigned to two subbands of the Ar–H_2O complex based on their observed chemistry, and on the fitted rotational constants (Table III). Two examples of these transitions along with computer generated stick spectra of each subband are shown in Figs. 3 and 4. The subband near 21 cm^{-1} (630 GHz), for which we have measured lines ranging from $P(20)$ to $R(17)$, and $Q(1)$ to $Q(20)$, has been assigned to the set of $K_a = 1 \leftarrow K_a = 0$ transitions across the tunneling levels in the ground vibrational state (i.e., $0^- \leftarrow 0^+$; the superscripts $+$, $-$ are used throughout this paper to label the lower and upper tunneling sublevels, respectively, of a given vibrational level). Lines ranging from $P(11)$ to $R(12)$ and $Q(1)$ to $Q(11)$ have been measured in another subband near 25 cm^{-1} (740 GHz), which is assigned to a $K_a = 0 \leftarrow K_a = 1$ transition from the 0^+ tunneling level to the $v_{b1} = 1^+$ state in a bending coordinate perpendicular to the hydrogen tunneling exchange motion. An energy level diagram showing the observed subband origins is shown in Fig. 5. Many other unassigned lines remain in the 7 cm^{-1} interval, some of which have been assigned to $(H_2O)_2$.[39]

TABLE I. Transitions measured in the 0^-, $K_a = 1 \leftarrow 0^+$, $K_a = 0$ subband of Ar–H_2O.

	Transition $v = 0^- \leftarrow v = 0^+$ $J'_{K'_a K'_c} \leftarrow J_{K_a K_c}$	Obs. freq. (MHz)	O − C (MHz)
1.	18 1 17 17 0 17	777 469.6	−0.7
2.	17 1 16 16 0 16	767 425.6	0.7
3.	16 1 15 15 0 15	757 587.8	0.6
4.	15 1 14 14 0 14	747 963.3	0.5
5.	14 1 13 13 0 13	738 555.8	−0.7
6.	13 1 12 12 0 12	729 371.1	−1.3
7.	12 1 11 11 0 11	720 414.6	0.4
8.	11 1 10 10 0 10	711 684.7	0.0
9.	10 1 9 9 0 9	703 187.0	0.2
10.	9 1 8 8 0 8	694 922.0	−0.8
11.	8 1 7 7 0 7	686 896.1	1.1
12.	7 1 6 6 0 6	679 104.3	−1.0
13.	6 1 5 5 0 5	671 556.6	0.8
14.	5 1 4 4 0 4	664 249.2	1.2
15.	4 1 3 3 0 3	657 184.1	0.4
16.	3 1 2 2 0 2	650 364.4	0.1
17.	2 1 1 1 0 1	643 791.6	0.0
18.	1 1 0 0 0 0	637 466.9	0.0
19.	20 1 20 20 0 20	654 302.2	0.9
20.	19 1 19 19 0 19	652 065.5	−0.6
21.	18 1 18 18 0 18	649 942.9	−1.0
22.	17 1 17 17 0 17	647 937.5	−0.5
23.	16 1 16 16 0 16	646 050.3	0.2
24.	15 1 15 15 0 15	644 281.8	0.6
25.	14 1 14 14 0 14	642 632.4	−1.2
26.	13 1 13 13 0 13	641 099.5	−0.2
27.	12 1 12 12 0 12	639 686.1	0.4
28.	11 1 11 11 0 11	638 388.0	0.2
29.	10 1 10 10 0 10	637 204.1	−0.5
30.	9 1 9 9 0 9	636 134.6	−0.2
31.	8 1 8 8 0 8	635 176.5	−0.2
32.	7 1 7 7 0 7	634 328.7	−0.3
33.	6 1 6 6 0 6	633 589.9	−0.4
34.	5 1 5 5 0 5	632 959.0	−0.4
35.	4 1 4 4 0 4	632 435.0	−0.1
36.	3 1 3 3 0 3	632 017.1	−0.1
37.	2 1 2 2 0 2	631 703.4	−0.8
38.	1 1 1 1 0 1	631 495.1	−0.7
39.	1 1 0 2 0 2	619 995.6	−0.2
40.	2 1 1 3 0 3	614 677.8	−0.1
41.	3 1 2 4 0 4	609 615.4	0.0
42.	4 1 3 5 0 5	604 810.7	0.8
43.	5 1 4 6 0 6	600 263.6	0.6
44.	6 1 5 7 0 7	595 976.8	0.5
45.	7 1 6 8 0 8	591 952.1	0.3
46.	8 1 7 9 0 9	588 191.4	0.2
47.	10 1 9 11 0 11	581 469.6	−0.2
48.	11 1 10 12 0 12	578 512.8	−0.4
49.	12 1 11 13 0 13	575 828.1	−0.5
50.	13 1 12 14 0 14	573 417.7	−0.5
51.	14 1 13 15 0 15	571 283.3	−0.4
52.	15 1 14 16 0 16	569 427.5	0.7
53.	16 1 15 17 0 17	567 848.6	−0.1
54.	17 1 16 18 0 18	566 550.2	0.3
55.	18 1 17 19 0 19	565 530.9	0.7
56.	19 1 18 20 0 20	564 787.7	−0.7

Rotational analysis

Rotational assignments of both subbands were straightforward since the progressions are easily identified, even in regions which were relatively congested. Initial measurements indicated that the effective rotational constant

TABLE II. Transitions measured in the $v_{b1} = 1^+, K_a = 0 \leftarrow 0^+, K_a = 1$ subband of Ar–H_2O.

	Transition $v_{b1} = 1^+ \leftarrow v = 0^+$ $J'_{K'_aK'_c} \leftarrow J_{K_aK_c}$	Obs. freq. (MHz)	O − C (MHz)
57.	13 0 13 12 1 12	833 331.3	0.0
58.	12 0 12 11 1 11	825 694.9	−0.1
59.	11 0 11 10 1 10	818 173.4	0.4
60.	10 0 10 9 1 9	810 769.9	0.1
61.	9 0 9 8 1 8	803 488.0	−1.1
62.	8 0 8 7 1 7	796 335.7	1.5
63.	7 0 7 6 1 6	789 307.3	−1.0
64.	6 0 6 5 1 5	782 413.3	−0.6
65.	5 0 5 4 1 4	775 654.5	0.8
66.	4 0 4 3 1 3	769 030.3	0.2
67.	3 0 3 2 1 2	762 545.5	0.0
68.	1 0 1 1 1 0	743 894.8	0.0
69.	2 0 2 2 1 1	743 783.7	−0.1
70.	3 0 3 3 1 2	743 619.4	−0.1
71.	4 0 4 4 1 3	743 404.2	0.0
72.	5 0 5 5 1 4	743 141.2	0.0
73.	6 0 6 6 1 5	742 834.5	0.1
74.	7 0 7 7 1 6	742 488.3	0.0
75.	8 0 8 8 1 7	742 107.9	0.3
76.	9 0 9 9 1 8	741 697.4	−0.4
77.	10 0 10 10 1 9	741 264.1	0.1
78.	11 0 11 11 1 10	740 811.7	0.0
79.	0 0 0 1 1 1	738 046.8	−0.3
80.	1 0 1 2 1 2	732 294.3	−1.0
81.	2 0 2 3 1 3	726 699.3	1.2
82.	3 0 3 4 1 4	721 259.0	0.6
83.	4 0 4 5 1 5	715 979.3	0.0
84.	5 0 5 6 1 6	710 863.4	−0.5
85.	6 0 6 7 1 7	705 915.4	0.1
86.	7 0 7 8 1 8	701 135.9	−0.8
87.	8 0 8 9 1 9	696 532.2	1.0
88.	9 0 9 10 1 10	692 101.5	−0.3
89.	10 0 10 11 1 11	687 851.2	0.0

TABLE III. Molecular constants determined in a simultaneous fit of both subbands.

S-reduced constants[a] (MHz)	
$v = 0^+$	
	$B^+ = 3014.765(76)$
	$C^+ = 2809.661(76)$
	$D_J^+ = 0.057\,77(34)$
	$D_{JK}^+ = -91.08(12)$
	$d_1^+ = -0.015\,60(66)$
	$H_J^+ = -0.024\,3(10) \times 10^{-3}$
	$H_{JK}^+ = -0.070\,2(16)$
	$h_1^+ = 0.007\,1(36) \times 10^{-3}$
	$L_J^+ = 0.008\,4(24) \times 10^{-6}$
	$L_{JK}^+ = 0.021\,9(72) \times 10^{-3}$
$v = 0^-$	
	$B^- = 2983.354(48)$
	$C^- = 2836.447(48)$
	$D_J^- = -0.013\,92(26)$
	$D_{JK}^- = -91.1$ (fixed)
	$d_1^- = -0.003\,712(64)$
	$H_J^- = -0.024\,7(42) \times 10^{-3}$
	$H_{JK}^- = -0.07$ (fixed)
	$h_1^- = 0.76(12) \times 10^{-6}$
$v_{b1} = 1^+$	
	$(B + C)/2 = 3026.55(18)$
	$D_J = 0.108\,8(12)$
	$H_J = -0.019\,0(46) \times 10^{-3}$
	$(A_{\text{eff}} + \Delta_{\text{tun}}) = 634\,301.65(50)$
	$(\omega_{b1} - \Delta_{01}/2 - A_{\text{eff}}) = 741\,038.48(66)$
Standard deviation = 670 kHz[b]	

[a] All error bars are 2σ.
[b] The correlation matrix is available from the authors upon request.

$(B + C)/2$ was approximately 3 GHz. For clusters of the type Ar_m–H_2O_n, only an Ar–H_2O complex could have a structure consistent with this value. Higher order clusters (trimers, tetramers, etc.) of the constituents which we deliberately placed in the jet would have a much smaller rotational constant, while water dimer has approximately twice the observed rotational constant.[3] The high intensity of the 21 cm^{-1} subband (S/N as high as 5000:1) made assignment to an impurity spectrum unlikely. As an additional test of the identity of the carrier of these lines, argon was replaced by nitrogen under identical conditions. Lines assigned to Ar–H_2O disappeared while the strongest of the remaining lines were still observable.

Observation of strong Q branches in both subbands suggested that the spectra arise from perpendicular transitions. The 21 cm^{-1} subband, for which we observe $R(0)$ and $P(2)$ but not $P(1)$, despite adequate sensitivity, is assigned as a $K_a = 1 \leftarrow K_a = 0$ subband. $P(10)$ was also not observed as it lies within 2 GHz of the 584 GHz laser line. The Q branch spacings confirm that this is a c-type band: Spacings between adjacent lines in the Q branch of a $K_a = 1 \leftarrow K_a = 0$ subband are given by $[\Delta_{01}(B + C)/2 \pm (B - C)/4]2J'$, where $\Delta_{01}(B + C)/2$ is the difference between the effective rotational constants in the upper and lower states. The asymmetry constant $(B - C)/4$ adds to $\Delta_{01}(B + C)/2$ for a b-type band is subtracted from it for a c-type band. Moreover, the high intensity and relative insensitivity to nozzle conditions indicates that this subband originates in a vibration–rotation–tunneling (VRT) level which cannot relax further by collisions in the nozzle expansion.

The 25 cm^{-1} subband, which is 15–40 times weaker, is much more sensitive to changes in the expansion conditions. In the initial scans through this region, some but not all of the low J lines in this subband were found, presumably because of this sensitivity. For this band we observe $P(1)$, but $R(0)$ and $R(1)$ are obscured by an atmospheric water absorption in the unpurged optical path. The observation of $P(1)$ establishes that the upper state is a $K_a = 0$ level and that the lower state is $K_a = 0$ or $K_a = 1$. The presence of a strong Q branch suggests that the lower state is $K_a = 1$. In this case, the Q branch spacing indicates that the band is b type. Both the observed chemistry and intensity suggest that this band does not originate in the ground VRT state. As discussed below in detail, we accordingly assign the lower state of each band to $K_a = 0$ and $K_a = 1$ of the 0^+ (lower) tunneling sublevel in the ground vibrational state. The upper states are assigned to two different VRT levels, 0^-, $K_a = 1$ and $v_{b1} = 1^+$, $K_a = 0$.

The data for both bands have been fit simultaneously to

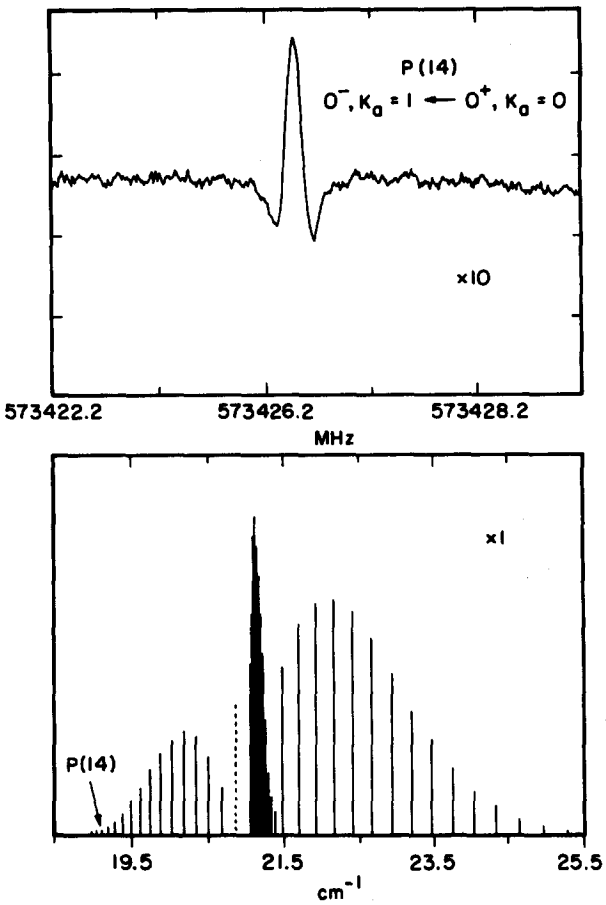

FIG. 3. A 10 MHz wide scan showing $P(14)$ (upper trace) of the 0^-, $K_a = 1 \leftarrow 0^+$, $K_a = 0$ subband of Ar–H_2O and a computer generated stick spectrum for an estimated rotational temperature of 6 K. The position of the missing $P(1)$ is shown as a dashed line. Relative intensities are for comparison with Fig. 4.

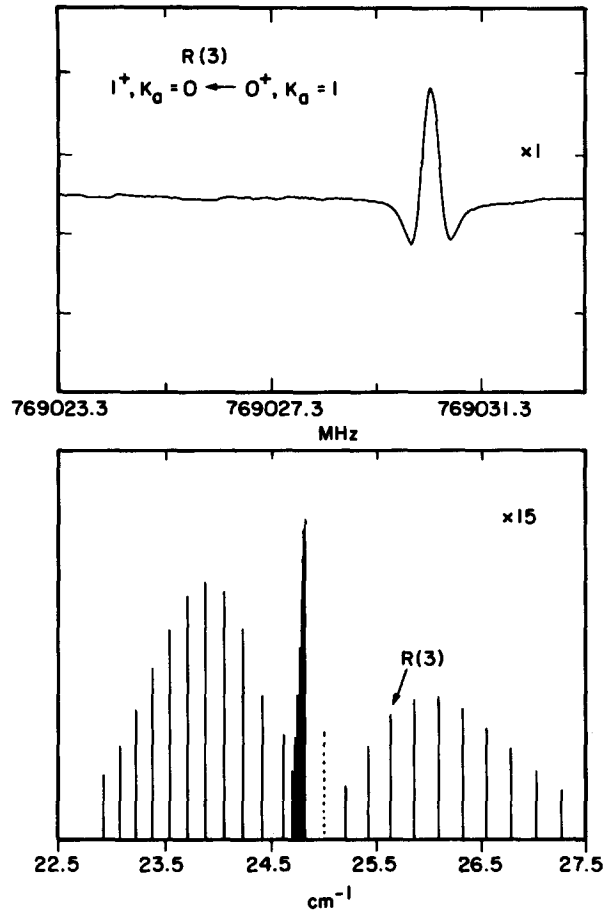

FIG. 4. A 10 MHz wide scan showing $R(3)$ of the $v_{b1} = 1^+$, $K_a = 0 \leftarrow 0^+$, $K_a = 1$ subband and a computer generated stick spectrum. The intensity of the strongest line in this simulation of the band is approximately 15 times weaker than the strongest line shown in Fig. 3.

a Watson S-reduced Hamiltonian. The resulting constants are shown in Table III. Constants for the 0^- level were determined by fixing D_{JK} and H_{JK} to the values determined for these constants in the 0^+ level, this was necessary since only one K_a level has been sampled in the 0^- manifold. The octic distortion terms L_J^+ and L_{JK}^+ were required to fit $J > 15$ lines to within the experimental uncertainty. Inclusion of an additional octic term L_J^- did not improve the fit. The standard deviation of the fit of 21 parameters to 89 lines is 670 kHz in good agreement with our estimate of the experimental uncertainty in the absolute frequencies of the lines. The sextic and octic distortion terms for each sublevel exhibited high correlations with each other, and in some cases with the quartic terms, but not with the constants of other sublevels.

The spectra obtained thus far yield accurate measurements of sums and differences of several of the VRT parameters; it is not possible, given the available data set, to separate the A rotational constant from the tunneling or vibrational frequencies. Many of the rotational parameters, although well determined, are effective linear combinations of low order parameters and higher order parameters which have been set to zero. Separation of these terms will require measurements of $K_a \geqslant 2$ sublevels. Effective rotation, $(B + C)/2$, and centrifugal distortion constants for all of the states involved in the two transitions are determined, yielding information on the center-of-mass separation of the argon and water and on the curvature of the potential function. The asymmetry constant $(B - C)/4$ of the complex and the centrifugal distortion of the asymmetry are determined for the 0^+ and 0^- tunneling sublevels, but not for the $v_{b1} = 1^+$ level, since for that state we have observed only a $K_a = 0$ stack. As will be discussed below, $(B - C)/4$ is considerably larger than can be explained by purely geometric, rigid rotor type contributions to the value of this constant and so it is not currently a useful parameter for structural calculations.

Vibrational assignment

We begin by assuming that on the time scale of one rotational period the two hydrogens are in symmetric environments. This may be the result of either the molecule possessing a C_{2v} equilibrium structure or of large amplitude tunneling motions about an asymmetric configuration which rapidly exchange the position of the two hydrogens. Based on this assumption we expect to find ortho and para forms of Ar–H_2O in the statistical ratio of 3:1. Only the lowest sublevels of the complex will have significant populations in the supersonic expansion which has a rotational tempera-

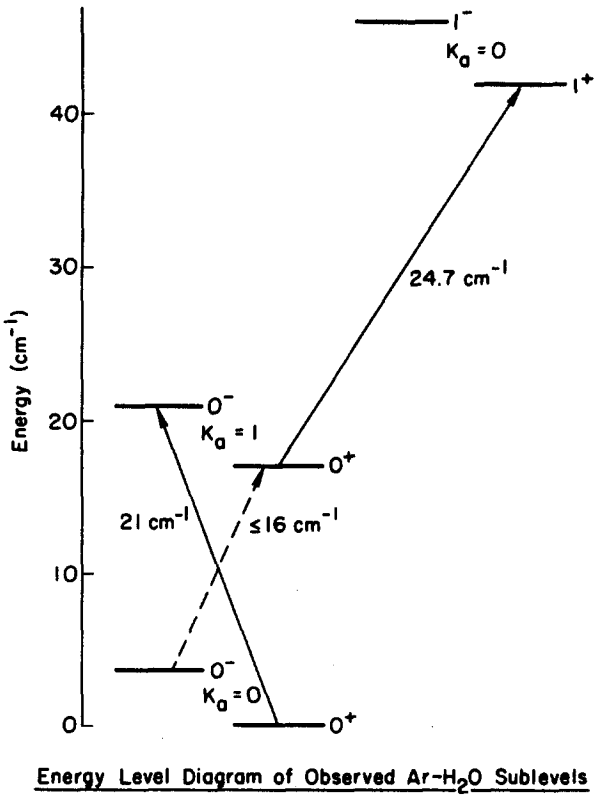

FIG. 5. Energy level diagram for Ar–H_2O depicting the observed subband origins (—solid lines) and the lower component of the rotation–tunneling doublet which has not been observed (--- dashed line). The $+/-$ superscripts are used to identify the lower and upper tunneling sublevels, respectively, of a given vibrational level. The $v = 1$ level is assigned as a bending vibrational mode normal to the tunneling coordinate.

ture near 5 K.[27] Depending on the vibrational spacing, the lowest ortho and para levels will be either the $K_a = 0$ and 1 levels of the ground vibrational state (these levels are spaced by at least 9.5 cm^{-1}, the minimum value of A for any geometric arrangement of an argon atom and a water molecule spaced by 3.7 Å) or the $K_a = 0$ levels of the ground state and of the first excited bending vibrational state. This is a standard result for molecules which possess C_{2v} symmetry. The first case will hold if the effective A rotational constant (A_{eff}) of the complex is less than ω_b, the lowest intermolecular bending frequency, and the second true if A_{eff} is greater than ω_b. In the case of rigid molecules one can easily rule out the second possibility as bending frequencies are hundreds of wave numbers while A rotational constants are tens of wave numbers at most. A summary of the nuclear spin states for the intermolecular vibrational levels of Ar–H_2O is given in Table IV.

For a molecule with C_{2v} symmetry $\Delta K_a = \pm 1$ transitions are forbidden for pure rotational transitions of the complex within the ground state or any excited vibrational or tunneling state, since they require a change of the nuclear spin state. Two $\Delta K_a = \pm 1$ bands of Ar–H_2O are observed: one a c-type band with $\Delta K_a = +1$ near 21 cm^{-1} GHz and one a b-type band with $\Delta K_a = -1$ near 25 cm^{-1}; these are therefore either rotation–tunneling or vibration–rotation transitions. The presence of a subband at 21 cm^{-1}, which originates in $K_a = 0$ is compelling evidence for the presence

TABLE IV. Nuclear spin symmetries for the van der Waals vibrations of Ar–H_2O. v_s labels the intermolecular stretch, v_b the intermolecular bending frequencies with n the number of quanta in each mode. The + and − signs label the lower and upper tunneling states, respectively.

Vibration–tunneling state	K_a even	K_a odd
$v = 0^+, v_s = n^+$	para	ortho
$v = 0^-, v_s = n^-$	ortho	para
$v_b = \text{even}^+$	para	ortho
$v_b = \text{even}^-$	ortho	para
$v_b = \text{odd}^+$	ortho	para
$v_b = \text{odd}^-$	para	ortho

of a very low frequency vibration, perhaps in the form of an internal rotation or a tunneling motion. $\Delta K_a = +1$ transitions originating in $K_a = 0$ will appear at a frequency given by $(A_{\text{eff}} \pm \omega_b)$. The effective A rotational constant for Ar–H_2O is expected to lie between 9.5 and 27.5 cm^{-1}; implying the existence of a vibrational level less than 11.5 cm^{-1} above the ground state.

As noted above, we assume that there are two equivalent minima in the PES of this complex corresponding to exchange of the positions of the two hydrogen atoms. Tunneling between these two minima is a likely choice for the assignment of the low frequency vibration but other possibilities must be considered. Evidence for tunneling between equivalent minima localized at the positions of the lone pairs on the oxygen atom has been presented for systems in which H_2O acts as a hydrogen bond acceptor.[4–6] For example, the tunneling frequency in H_2O–HF was determined to be approximately 65 cm^{-1}.[4] This complex is much more strongly bound ($D_e \simeq 10$ kcal/mol[43]) than is Ar–H_2O ($D_e \simeq 0.4$ kcal/mol[34]), indicating that if tunneling is occurring between identical Ar–OH_2 configurations [Fig. 1(c)], then it will be even higher in frequency than the 65 cm^{-1} H_2O–HF splitting. Tunneling is not observed in H_2O–C_2H_2[7] in which water also acts as a hydrogen bond acceptor. In this dimer the dissociation energy $D_e \simeq 2$–3 kcal/mol[44] is intermediate between that of H_2O–HF and Ar–H_2O. Interchange of the hydrogens is thus the most likely candidate for a low frequency ($\omega < 11$ cm^{-1}) tunneling motion.

By convention, vibrational levels are labeled by the quantum numbers $v = 0,1,2,3,...$ if the $v = 0$ level is above any barriers in the potential of the relevant coordinate and the level spacing changes in a monotonic way. These same levels are given the labels $v = 0^{\pm}, 1^{\pm},...$ if the barrier is higher than the zero-point level and the reaction coordinate between equivalent minima is not equivalent to an internal rotational motion. This would be the case, e.g., if the equilibrium structure of Ar–H_2O were that of Fig. 1(a), a linear hydrogen bonded structure, and exchange between the two possible hydrogen bonded configurations proceeded via a planar C_{2v} intermediate. If on the other hand, exchange proceeded via internal rotation of the H_2O subunit about its axis of symmetry then the preferred labeling of the vibrational levels would be $v = 0_a, 0_b, 1_a, 1_b,...$ where a and b would refer to different internal rotor substates.

We choose to use the labeling scheme associated with an inversion tunneling path to describe the low-lying vibrational levels. The label ω_b, which we have thus far used to denote the lowest bending vibrational frequency, is replaced with the label Δ_{tun}, which identifies the lowest pair of levels as a tunneling doublet. The data thus far available are insufficient to indicate whether this is a more appropriate choice than the use of internal rotor labeling, although it does suggest that one of these two is a better choice than a barrier-free labeling scheme.

The 21 cm^{-1} band may be assigned as either the 0^-, $K_a = 1 \leftarrow 0^+$, $K_a = 0$ (the lower solid line in Fig. 5) with a subband origin at $(A_{eff} + \Delta_{tun})$ or as the 0^+, $K_a = 1 \leftarrow 0^-$, $K_a = 0$ (dashed line in Fig. 5) with a subband origin at $(A_{eff} - \Delta_{tun})$. The first of these transitions is among para levels and the second among ortho levels; hence the relative intensities of the two choices differ by a factor of 3. The large ambiguity in the value of A makes it difficult to definitively determine which of these two possible assignments is correct. In order to demonstrate the range of possible values for the rigid rotor contribution to the A rotational constant in Fig. 1 we show several structures which span the range from what is nearly the smallest A value of 10 cm^{-1} [Fig. 1(c)] to the largest value possible for a rigid structure of 27.5 cm^{-1} [Fig. 1(b)]. The choice of the $(A_{eff} - \Delta_{tun})$ assignment requires A to be near this maximum. Failure to observe a corresponding tunneling partner at $(A_{eff} + \Delta_{tun})$ below 27.5 cm^{-1}, for which one expects a P branch width of at least 1 cm^{-1} (for the 21 cm^{-1} band the P branch is 2.3 cm^{-1} wide) give $(A_{eff} + \Delta_{tun}) \geqslant 28.5$ cm^{-1}, and $A_{eff} \geqslant 24.8$ cm^{-1}. Internal rotation may increase the magnitude of the A constant from its rigid rotor value and this number is at least possible for a rigid structure. Nonetheless, it is close to the largest reasonable value for A and corresponds to an unlikely planar structure for the molecule with the symmetry axis of the water subunit perpendicular to the Ar–O axis [Fig. 1(b)]. The alternative assignment of the 21 cm^{-1} subband is across the tunneling doublet from the lower to upper tunneling states, 0^-, $K_a = 1 \leftarrow 0^+$, $K_a = 0$. The failure to observe a tunneling partner to this band at frequencies above 20 cm^{-1}, given an expected R branch width of 4 cm^{-1} (for the observed band the R branch is 5 cm^{-1} wide) sets a maximum value for $(A_{eff} - \Delta_{tun})$ of 16 cm^{-1}, and sets an upper limit to A_{eff} of 18.5 cm^{-1}. This assignment puts A in a range which is compatible with some of the most chemically intuitive structures (e.g., a linear hydrogen bonded structure or a C_{2v} hydrogen bonded structure), as well as with a structure which is analogous to the observed Ar–H_2S structure, for which A of Ar–H_2O would be 17 cm^{-1} [Fig. 1(d)].

We now consider the assignment of the 25 cm^{-1} subband. We have shown that this is a b-type subband originating in a $K_a = 1$ level, which, based on the constants obtained from the rotational analysis, is not the same as the upper state of the 21 cm^{-1} transition. The assignment of the two bands is not independent, since in the model thus far outlined one of the two postulated 0^+, 0^-, $K_a = 1$ levels must belong to each transition. The assignment of the 21 cm^{-1} band as 0^-, $K_a = 1 \leftarrow 0^+$, $K_a = 0$ determines that the 25 cm^{-1} subband originates in 0^+, $K_a = 1$, with the converse true for the alternative assignment. The term energy of this state is $(A_{eff} + \Delta_{tun})$, $(A_{eff} - \Delta_{tun})$, or if $\Delta_{tun} \geqslant A_{eff}$, it is $(\Delta_{tun} - A_{eff})$. We have already established above that these energies are either $E \geqslant 28.5$ cm^{-1} or $E \leqslant 16$ cm^{-1}. In a jet with a 5 K rotational temperature, which is approximately the rotational temperature of the expansion used in this study,[27] observation of a level at 28 cm^{-1} above the lowest levels is unlikely, although if the transition moment were sufficiently strong, it might be possible given the current level of sensitivity. For example, the high J rotational lines observed in the 21 cm^{-1} band are 40 cm^{-1} above the ground state. In the shock boundary of the two-dimensional jet higher temperatures have been observed in our previous study of Ar–HCl,[27] molecules in this region of the expansion could be contributing to the signals observed in this work. The high J lines of the 25 cm^{-1} band originate approximately 14 cm^{-1} above the $K_a = 1$, $J = 1$ energy and have a total excitation energy of either $E \leqslant 30$ cm^{-1} for the assignment to 0^+, $K_a = 1$ or $E \geqslant 52$ cm^{-1} for assignment to the 0^-, $K_a = 1$ state. A total excitation energy of 30 cm^{-1} seems more reasonable, particularly since assignment of the lower state of the 21 cm^{-1} band to the 0^+, $K_a = 1$ implies that the 25 cm^{-1} transition is among ortho levels, with the three-fold nuclear spin degeneracy increasing its intensity relative to the 21 cm^{-1} band. The alternative assignment (to 0^-, $K_a = 1$) would be three times less intense since it is among para levels. Because of the dual requirement of high excitation energy and reduced intensity we can probably rule out assignment of the lower state of this band to the 0^-, $K_a = 1$ level and assign it instead to 0^+, $K_a = 1$. This yields additional evidence that the 21 cm^{-1} band is due to the transition 0^-, $K_a = 1 \leftarrow 0^+$, $K_a = 0$.

Up to this point we have not discussed the assignment of the vibrational level in which the 25 cm^{-1} subband terminates. This vibrational level is (25 $cm^{-1} + A_{eff}$) above the lower tunneling sublevel (0^+, $K_a = 0$). Three VRT transitions with $\Delta K_a = -1$ subbands seem probable: (1) to $v_{b1} = 1^+$, the lower tunneling sublevel of a bending motion perpendicular to the hydrogen exchange tunneling coordinate; (2) to $v_{b2} = 1^+$, the lower tunneling sublevel of the first vibrational transition in the tunneling (or internal rotation) coordinate, and (3) to the upper tunneling sublevel of the van der Waals stretching vibration $v_s = 1^-$ (the subscripts b 1 and b 2 are chosen only to identify the two bending vibrations).

For the tunneling coordinate, the energy of $v = 1^\pm$ might be expected to be higher than that of the observed level. For a slightly hindered internal rotor, the spacing between the $0^\pm$ and the $1^\pm$ levels will be approximately the spacing between successive even or odd rotational levels of the free monomer. If rotation about the c axis of H_2O were the tunneling path, e.g., this would correspond to the difference in energy between the 0_{00} and 2_{02} or 1_{01} and 3_{03} levels of the free H_2O monomer—more than 70 cm^{-1}. In addition, the 25 cm^{-1} band is a b-type band, whereas the rotation–tunneling band is c type. It is difficult to rationalize why the projection of the dipole derivative would change from along the c axis to along the b axis in the transition to $v = 1$. Nonetheless the ambiguity surrounding the tunneling path does not allow us to completely rule out assignment of the upper

state to $v_{b2} = 1^+$.

We can more confidently eliminate consideration of the van der Waals stretching vibration. Transitions to the stretch are predominantly *a* type (parallel), although angular-radial coupling may result in *b* or *c* components of the dipole derivative. Transitions to the $v_s = 1^-$ would require a perpendicular dipole derivative and therefore are likely to be weak. In addition, $(B + C)/2$ in the $1^+, K_a = 0$ state, is 4% larger than $(B + C)/2$ in the $0^+, K_a = 0$ state, implying the subunits are closer together, not further apart as would be expected for a stretch. This fact suggests that the motion involved is a bending motion which moves the hydrogens to allow closer approach of the argon and oxygen. For comparison, in Ar–HCl, *B* in both of the lowest bending states is 4% larger than in the ground state, but *B* for $v = 1$ of the van der Waals stretch is 7% smaller than *B* in the ground state.[21–23] The first of the suggested possibilities is most favorable; we assign the spectrum to the transition $v_{b1} = 1^+$, $K_a = 0 \leftarrow v = 0^+, K_a = 1$. The band origin for this band appears at the difference $(\omega_{b1} - \Delta_{01}/2 - A_{\text{eff}})$, with Δ_{01} being the difference in the tunneling splitting in the upper and lower states. A diagram of the observed transitions is shown in Fig. 5.

Based on the interval over which we have continuously scanned, 20–27.5 cm^{-1}, and the failure to observe other subbands in this region, the range of possible values for A_{eff}, the tunneling splitting, and the vibrational frequency ω_{b1} can be determined. These values will help to constrain the geometry of the complex and aid in the prediction of the positions of other subbands. The relative intensity of the two observed subbands gives an estimate of the excitation energy of the $0^+, K_a = 1$ level above the lowest level of the same nuclear spin symmetry, the $0^-, K_a = 0$ level, assuming the transition moments of the different subbands to be nearly the same. The subband at 25 cm^{-1} is approximately 15–40 times weaker than the 21 cm^{-1} subband, based on the relative intensity of several of the low-*J* lines. Taking into account the fact that it has three times the nuclear spin weight gives a normalized intensity reduced by 45–120. For a 3 to 7 K expansion temperature this corresponds to an excitation energy of 16 ± 8 cm^{-1}. The upper limit to $(A_{\text{eff}} - \Delta_{\text{tun}})$, the excitation energy, was shown earlier to be 16 cm^{-1}. Combining these two sets of constraints gives the tunneling splitting Δ_{tun} in the range of 2.5–6.5 cm^{-1}, A_{eff} between 14.5 and 18.5 cm^{-1}, and $(\omega_{b1} - \Delta_{01}/2)$ between 39 and 43 cm^{-1}.

Geometry

In order to completely specify the equilibrium or vibrationally averaged structure of Ar–H_2O three coordinates must be given. We take these to be $R_{\text{c.m.}}$, the distance between the centers of mass of the argon atom and the H_2O subunit θ, the angle between the symmetry axis of the H_2O subunit and the *a* axis of the complex, and χ, the angle of rotation of the H_2O subunit about its symmetry axis, which is measured from the reference planar configuration. Figure 1 shows θ and χ for some Ar–H_2O geometries; these were chosen to display the full range of possible values for the rigid rotor contribution to the *A* rotational constant and for comparison with the structures which have been determined for other H_2O–X, and H_2S–X complexes. If the effects of large amplitude vibrational motions could be neglected then the combination of the fitted constants *B* and *C* as well as the limited range of *A* values which is compatible with the existing data set would be sufficient constraints on these three coordinates to enable a qualitative understanding of the geometry of the molecule to be achieved. Because of strong mixing of vibration and rotation, however, the rotational constants determined do not solely describe geometrical relations of the atoms in the complex but reflect the nature of the internal motions as well. No simple method of deconvoluting these effects is currently available. One example of the problem is the large size of the asymmetry constant: $(B - C)/4$ is about ten times larger than can be accounted for by any rigid structure which reproduces $(B + C)/2$, rendering it impossible to use the conventional formulas in the determination of a structure. Similar results have been found for several van der Waals molecules including $(H_2O)_2$[2] and the second row homolog of Ar–H_2O, the Ar–H_2S complex. For Ar–H_2S,[36] $(B - C)/4$ is approximately three times larger than can be accounted for by the average structure determined for the complex.

The *A* rotational constant is also expected to be significantly affected by large amplitude internal motions. The time scale of rotation about the *a* axis, which almost exclusively involves the motion of hydrogen atoms, is on the same order as that of the van der Waals vibrations allowing large coupling between these degrees of freedom. This difficulty is further complicated by the selection rules, which forbid $\Delta K_a = \pm 1$ transitions for pure rotation, thus making direct measurement of A_{eff} in the two different sublevels impossible. Only the average values of A_{eff} and the tunneling splitting, Δ_{tun} in the two states may be determined, although A_{eff} may actually be quite different in the 0^+ and 0^- tunneling sublevels.

Despite these reservations some structural information may be gleaned from the available data. As has been discussed by Klemperer *et al.* in many of their studies of van der Waals molecules (e.g., Ref. 45), in the limit of free rotation the measured rotational constant $(B + C)/2$ approximates the pseudodiatomic rotational constant *B*. Within this approximation we obtain $R_{\text{c.m.}} = 3.75$ Å for the $0^+, K_a = 0$ level. Uncertainty on the order of 0.1 Å arises from our incomplete knowledge of the orientation of the H_2O subunit within the complex. This bond length is intermediate between those of Ar–HF ($R_{\text{c.m.}} = 3.51$ Å[46]) and of Ar–NH_3 ($R_{\text{c.m.}} = 3.84$ Å[45]). The bond lengths of these and several other argon complexes are given in Table V. Our result for Ar–H_2O is quite different from the 2.9 Å result suggested by the molecular beam scattering experiments.[34,35]

From our estimate of the effective *A* rotational constant, we can place constraints on the angles θ and χ. If internal rotation does not contribute more than 10%–15% to the effective *A* rotational constant then the rigid rotor contribution to A_{eff}, which is what relates to a vibrationally averaged structure, ranges from 12–21 cm^{-1}. This is an extremely weak constraint which only suggests that for near perpendicular geometries ($60° \leqslant \theta \leqslant 120°$), extremes of χ near 0° and 90°

TABLE V. Stretching force constants and center of mass separations for complexes of argon with first and second row hydrides in their ground vibrational states.

	k_s (mdyn/Å)	$R_{c.m.}$ (Å)	Reference
Ar–HF	0.0139	3.51	45
Ar–H_2O	0.0134	3.75	[a]
Ar–NH_3	0.0085	3.84	44
Ar–HCl	0.0117	4.00	46
Ar–H_2S	0.0055	3.98	35

[a] Present work.

are not likely. Acceptable values of χ fall between 15° and 60°. Even though only a small range of possible angles is eliminated by these constraints, the tetrahedrally bonded Ar–OH_2 configuration can be ruled out. For this structure, shown in Fig. 1(c), $\theta = 109.5°$ and $\chi = 90°$. Vibrationally averaged rms deviations from this structure of up to 30° do not diminish the evidence against this equilibrium structure, although larger deviations would.

Using the Kratzer relation $k_s = \mu B_{\text{eff}}^3 (4\pi)^2 / D_J$, with μ, the reduced mass of the complex, we can derive the harmonic stretching force constant, within the pseudodiatomic approximation.[45] The resulting stretching force constant in the 0^+, $K_a = 0$ level is 0.0134 mdyn/Å. This corresponds to a harmonic stretching frequency of 40 cm^{-1}. For comparison, stretching force constants of related complexes are given in Table V. It is apparent that the Ar–H_2O stretching force constant is similar to that of Ar–HF and Ar–HCl but the van der Waals bond is much stiffer than that of either Ar–NH_3 or Ar–H_2S.

DISCUSSION

A large number of weakly bound complexes containing water have now been studied extensively by microwave spectroscopy, as have several H_2S analogs.[2–17] The structures determined have all been rationalized in terms of the Lewis acid-base chemistry of the two subunits. The binding energies and stretching force constants in all these complexes are substantially larger than those of the Ar–H_2O complex, making generalization to the geometrically simpler atom–triatom system difficult. The complex internal dynamics involved in hydrogen exchange motions have made it unusually difficult to gain insight into the structures and forces operating in these complexes. Since Ar–H_2O is the most weakly bound among the measured H_2O–X dimers, it might be expected to be analogous to the next most weakly bound complex H_2O–C_2H_4,[10] which has a stretching force constant $k_s = 0.046$ mdyn/Å—four times that of Ar–H_2O. The structure of this complex is a hydrogen bonded configuration with the H_2O bound into the electron rich π system of ethylene. This lends some support for a hydrogen bonded equilibrium structure for Ar–H_2O. Nonetheless, significant ambiguity is present and prior studies of H_2O–X dimers do not lead to a clear prediction for the structure of Ar–H_2O.

Argon has been shown to act as a Lewis base in a number of complexes including Ar–HX (X = F,[46] Cl[47]), and Ar–CO_2,[48] thus it might be expected that the Ar–H_2Y (Y = O,S) complexes would be hydrogen bonded. In the Ar–H_2S complex a structure which is incompatible with this model was determined from microwave spectroscopy of a $K_a = 0$ triplet nuclear spin level.[36] In the notation used to describe the Ar–H_2O spectrum in this work, this triplet level would correspond to the 0^-, $K_a = 0$ tunneling sublevel of the Ar–H_2S dimer. Since there are considerable similarities in the potential energy surfaces and geometries of the Ar–HF and Ar–HCl molecules, one might expect that such comparisons between Ar–H_2S to Ar–H_2O would be reasonable. Anomalies in the stretching force constants of various Ar–H_nX complexes render such generalizations dubious, however. From Table V it can be seen that there is a pronounced drop in stretching force constant moving to the left across the Periodic Table from Ar–H_2O to Ar–NH_3 and from Ar–HCl to Ar–H_2S. If stretching force constants alone were an indicator of the structure and degree of nonrigidity of weakly bound complexes, then Ar–H_2O would be expected to be a linear hydrogen bonded complex, as are Ar–HCl and Ar–HF, and not necessarily similar in structure to the Ar–H_2S complex. Ar–H_2S would then be expected to be a nearly free internal rotor, as is Ar–NH_3. Experimental results actually suggest, however, that Ar–H_2S is not a free internal rotor.[36]

Lovas *et al.*[49] recently measured the microwave spectrum of the 0^+ level of Ar–H_2O at frequencies within 300 kHz of those predicted, with the constants reported and obtained in this work. Evidence was obtained for a very small dipole moment along the *a* axis. This result strongly implies that the C_{2v} axis of the H_2O subunit is nearly perpendicular to the *a* axis of the complex or that the complex is a near free internal rotor, like Ar–NH_3. Further studies are clearly needed to unequivocally establish the structure and internal dynamics of Ar–H_2O.

ACKNOWLEDGMENTS

This work was supported by the Director, Office of Energy Research, Office of Basic Energy Sciences, Chemical Sciences Division of the U. S. Department of Energy under Contract No. DE-AC03-76SF00098. The FIR laser system was funded by the National Science Foundation (Grant No. CHE-8612296) and by the Army Research Office University Research Instrumentation Program (Grant No. DAAL03-86-G-0184).

[1] G. T. Fraser, D. D. Nelson, K. I. Peterson, and W. Klemperer, J. Chem. Phys. **84**, 2472 (1986), and references therein.
[2] L. H. Coudert, F. J. Lovas, R. D. Suenram, and J. T. Hougen, J. Chem. Phys. **87**, 6290 (1987).
[3] J. A. Odutola, T. A. Hu, D. Prinslow, S. E. Odell, and T. R. Dyke, J. Chem. Phys. **88**, 5352 (1988); T. R. Dyke, K. M. Mack, and J. S. Muenter, *ibid.* **66**, 498 (1977).
[4] Z. Kisiel, A. C. Legon, and D. J. Millen, Proc. R. Soc. London Ser. A **381**, 419 (1980), and references therein.
[5] A. C. Legon and L. C. Willoughby, Chem. Phys. Lett. **95**, 449 (1983).
[6] A. J. Fillery-Travis, A. C. Legon, and L. C. Willoughby, Chem. Phys. Lett. **98**, 369 (1983).
[7] K. I. Peterson and W. Klemperer, J. Chem. Phys. **81**, 3842 (1984).
[8] K. I. Peterson and W. Klemperer, J. Chem. Phys. **80**, 2439 (1984).
[9] P. Herbine and T. R. Dyke, J. Chem. Phys. **83**, 3768 (1985).
[10] K. I. Peterson and W. Klemperer, J. Chem. Phys. **85**, 725 (1986).
[11] K. I. Peterson, G. T. Fraser, D. D. Nelson, Jr., and W. Klemperer, in

Comparison of Ab Initio Quantum Chemistry with Experiments for Small Molecules, edited by R. J. Bartlett (Reidel, Dordrecht, 1985), pp. 217–244.
[12]F. J. Lovas, R. D. Suenram, G. T. Fraser, C. W. Gillies, and J. Zozom, J. Chem. Phys. **88**, 722 (1988).
[13]R. Viswanathan and T. R. Dyke, J. Chem. Phys. **77**, 1166 (1982).
[14]L. C. Willoughby, A. J. Fillery-Travis, and A. C. Legon, J. Chem. Phys. **81**, 20 (1984).
[15]E. J. Goodwin and A. C. Legon, J. Chem. Soc. Faraday Trans. 2 **80**, 51 (1984).
[16]A. I. Jaman and A. C. Legon, J. Mol. Struct. **145**, 261 (1986).
[17]E. J. Goodwin and A. C. Legon, J. Chem. Soc. Faraday Trans. 2 **80**, 1669 (1984).
[18]K. W. Jucks and R. E. Miller, J. Chem. Phys. **88**, 2196 (1988).
[19]A. R. W. McKellar, Faraday Discuss. Chem. Soc. **73**, 89 (1982).
[20]U. Buck, H. Meyer, and R. J. Leroy, J. Chem. Phys. **80**, 5589 (1984).
[21]R. L. Robinson, D. Ray, D.-H. Gwo, and R. J. Saykally, J. Chem. Phys. **87**, 5149 (1987).
[22]R. L. Robinson, D.-H. Gwo, and R. J. Saykally, J. Chem. Phys. **86**, 5211 (1987); Mol. Phys. **63**, 1201 (1988).
[23]R. L. Robinson, D.-H. Gwo, and R. J. Saykally, J. Chem. Phys. **87**, 5156 (1987).
[24]L. S. Danielson, M. Keil, and P. J. Dunlop, J. Chem. Phys. **88**, 4128 (1988).
[25]J. M. Hutson, J. Chem. Phys. (submitted).
[26]J. M. Hutson and B. J. Howard, Mol. Phys. **45**, 769 (1982).
[27]K. L. Busarow, G. A. Blake, K. B. Laughlin, R. C. Cohen, Y. T. Lee, and R. J. Saykally, J. Chem. Phys. **89**, 1268 (1988).
[28]C. M. Lovejoy, M. D. Schuder, and D. J. Nesbitt, J. Chem. Phys. **85**, 4890 (1986).
[29]K. Watanabe and H. C. Andersen, J. Phys. Chem. **90**, 795 (1986).
[30]C. Pangali, M. Rao, and B. J. Berne, J. Chem. Phys. **71**, 2975 (1979).
[31]M. Losonczy, J. W. Moskowitz, and F. H. Stillinger, J. Chem. Phys. **59**, 3264 (1973).
[32]H. Lischka, Chem. Phys. Lett. **20**, 448 (1973).
[33]W. Kolos, G. Corongiu, and E. Clementi, Int. J. Quantum Chem. **17**, 775 (1980).
[34]R. W. Bickes, Jr., G. Duquette, C. J. N. van den Meijdenberg, A. M. Rulis, G. Scoles, and K. M. Smith, J. Phys. B **8**, 3034 (1975).
[35]R. Brooks, F. Kalos, and A. E. Grosser, Mol. Phys. **27**, 1071 (1974).
[36]R. Viswanathan and T. R. Dyke, J. Chem. Phys. **82**, 1674 (1985).
[37]G. A. Blake, K. L. Busarow, R. C. Cohen, K. B. Laughlin, Y. T. Lee, and R. J. Saykally, J. Chem. Phys. (submitted).
[38]K. L. Busarow, R. C. Cohen, G. A. Blake, K. B. Laughlin, Y. T. Lee, and R. J. Saykally (in preparation).
[39]K. B. Laughlin, G. A. Blake, R. C. Cohen, D. C. Hovde, and R. J. Saykally, Philos. Trans. R. Soc. London Ser. A **324**, 109 (1988).
[40]K. B. Laughlin, Ph.D. thesis, University of California, Berkeley, 1988.
[41]K. Veeken and J. Reuss, Appl. Phys. B **38**, 117 (1985).
[42]M. Ignuscio, G. Moruzzi, K. M. Evenson, and D. A. Jennings, J. Appl. Phys. **60**, R161 (1986).
[43]M. M. Szczesniak, S. Scheiner, and Y. Bouteiller, J. Chem. Phys. **81**, 5024 (1984).
[44]M. J. Frisch, J. A. Pople, and J. E. Del Bene, J. Chem. Phys. **78**, 4063 (1983).
[45]D. D. Nelson, Jr., G. T. Fraser, K. I. Petersen, K. Zhao, W. Klemperer, F. J. Lovas, and R. D. Suenram, J. Chem. Phys. **85**, 5512 (1986).
[46]T. A. Dixon, C. H. Joyner, F. A. Baiocchi, and W. Klemperer, J. Chem. Phys. **74**, 6539 (1981).
[47]S. E. Novick, K. C. Janda, S. L. Holmgren, M. Waldman, and W. Klemperer, J. Chem. Phys. **65**, 1114 (1976).
[48]J. M. Steed, T. A. Dixon, and W. Klemperer, J. Chem. Phys. **70**, 4095 (1979).
[49]F. J. Lovas (private communication).